Acta Acustica 2026, **10**, 27

https://doi.org/10.1051/aacus/2026028

Available online at:
https://acta-acustica.edpsciences.org

SHORT COMMUNICATION OPEN ACCESS

On the influence of the stress gradient on propagation behaviour of Rayleigh waves

Marcel Ruetz[1,*], Thomas Antretter[2], and Hans-Peter Gänser[1]

[1]Materials Center Leoben Forschung GmbH, Vordernbergerstraße 12, 8700 Leoben, Austria
[2]Chair of Mechanics, Montanuniversität Leoben, Franz-Josef Straße 18, 8700 Leoben, Austria

Received 13 October 2025, Accepted 13 March 2026

Abstract – This short communication presents a new combined numerical and signal processing based analysis of the influence of stress gradients on Rayleigh wave propagation. The method uses finite element simulations based on the hyperelastic Murnaghan model, to caputure the acoustoelastic effect, and an adapted coda Wave Interferometry (CWI) technique to quantify time shift and stretch of Rayleigh wave signals. It is shown that the stress gradient alters both wave velocity and wave shape. While tensile stress reduces wave velocity, a stress gradient can counteract this effect and even enhance the propagation velocity. The combined evaluation of time shift and stretch allows an effective description of the influence of both surface stress and stress gradient on the wave propagation.

Keywords. Rayleigh wave, Coda wave interferometry (CWI), Finite element analysis

1 Introduction

Rayleigh waves are well suited for near-surface residual stress assessment because their effective penetration depth scales with wavelength and can thus be tuned by the excitation frequency. The observed stress dependence of propagation velocity originates from the acoustoelastic effect, which requires a nonlinear constitutive description (e.g., the Murnaghan model) rather than linear elasticity [1–5]. Since Crecraft's pioneering work [6], ultrasonics can be used for (residual) stress detection, often with body-wave configurations such as LCR waves in welded or cast components [7, 8]. However, real engineering parts typically exhibit stress gradients. These gradients induce a depth-dependent wave velocity and, consequently, waveform distortion (dispersion), which can bias classical time-of-flight (ToF) evaluations that rely on velocity shift alone [9–12].

This short communication addresses the questions of how and how strongly stress gradients influence Rayleigh wave propagation, and how this influence can be robustly separated from the influence of the stress. Our approach combines (i) a numerical study using the isotropic hyperelastic Murnaghan model in ABAQUS/Explicit to systematically vary surface stress and gradient, with (ii) an adapted coda-wave interferometry (CWI) procedure applied directly to the measured Rayleigh wave [13, 14]. The method extracts two independent observables from a single surface trace: shift (time delay ⇒ velocity change) and stretch (temporal dilation ⇒ gradient-induced dispersion). The numerical results indicate that increasing tensile stress reduces Rayleigh wave velocity, whereas increasing stress gradient raises the apparent velocity because the average stress within the penetration depth decreases. Gradients produce measurable dispersion, particularly at lower frequencies where the penetration depth is larger. We condense these trends into compact regression relations, introducing the concept of effective measured stress.

2 Materials and methods

2.1 Material model and FE setup

Rayleigh wave propagation is simulated in ABAQUS/Explicit using the isotropic, weakly nonlinear hyperelastic Murnaghan model implemented via a Fortran `VUMAT` subroutine. Second-order (Lamé) constants are $\lambda = 90\,900\,\text{MPa}$ and $\mu = 78\,000\,\text{MPa}$; third-order (Murnaghan) constants are $\nu_1 = 358\,000\,\text{MPa}$, $\nu_2 = -265\,000\,\text{MPa}$, $\nu_3 = -182\,000\,\text{MPa}$. The elastic potential U for the Murnaghan model as function of the Green–Lagrange strain tensor $\mathbf{E}$ is given by:

*Corresponding author: marcel.ruetz@mcl.at

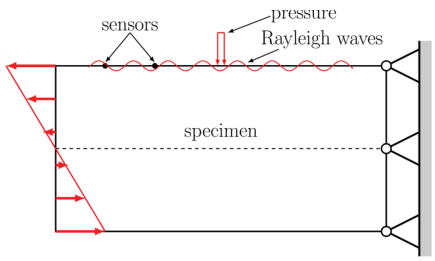

Figure 1. Sketch of the numerical model with the load, support, wave initiation and virtual sensors for detecting the elastic wave.

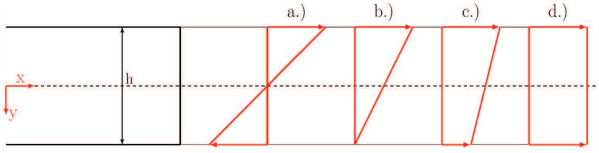

Figure 2. Variation of the stress gradient. (a) Pure bending stress ($\chi = 2/h$), (b) Bending stress superimposed with tensile stress ($\chi = 1/h$), (c) Bending stress superimposed with tensile stress ($\chi = 1/(2h)$), (d) Pure tensile stress ($\chi = 0$).

$$U = \frac{1}{2}\lambda\,(\operatorname{tr}\mathbf{E})^2 + \mu\operatorname{tr}(\mathbf{E}^2) + \frac{1}{3}\nu_1\,(\operatorname{tr}\mathbf{E})^3 + \nu_2\,(\operatorname{tr}\mathbf{E})\operatorname{tr}(\mathbf{E}^2) + \nu_3\operatorname{tr}(\mathbf{E}^3). \tag{1}$$

The domain is a cuboid solid meshed with C3D8R elements; to resolve the wavefield, the element edge length is set to $a = \lambda_{\mathrm{RW}}/10$, where λ_{RW} denotes the wave length of the Rayleigh wave. Different stress fields are introduced in a preceding quasi-static step as a depth-dependent normal stress $\sigma(y)$ defined by an analytical field; the subsequent dynamic step simulates wave excitation and reception. A surface pressure $p(t)$ over a small patch excites the Rayleigh wave with time history (burst). Two virtual surface sensors on the FE model, separated by $\Delta x = 100\,\mathrm{mm}$, record out-of-plane particle velocity with a sampling rate $\geq 20\,f$. The numerical model is shown in Figure 1.

2.2 Stress states and gradients

We study surface stresses σ_1 and linear depth gradients $\mathrm{d}\sigma/\mathrm{d}y$ within $|\sigma_1| \leq 600\,\mathrm{MPa}$ and $|\mathrm{d}\sigma/\mathrm{d}y| \leq 60\,\mathrm{MPa/mm}$. Figure 2 shows the investigated stress distributions. For characterisation of the different stress distributions, Siebel's normalised stress gradient χ [15] is used.

$$\chi = \left|\frac{1}{\sigma_1}\frac{\mathrm{d}\sigma}{\mathrm{d}y}\right|. \tag{2}$$

2.3 Adapted coda-wave interferometry (CWI)

To robustly extract small velocity changes and gradient-induced waveform distortions, an adapted CWI is applied directly to the recorded Rayleigh wave signal. After band-pass filtering around f, the relevant portion of the waveform is divided into short windows $[t_1, t_2]$, and for each window the normalised cross-correlation (Eq. (4)) is evaluated.

$$R^{(t_1,t_2)}(t_s) = \frac{\int_{t_1}^{t_2} u_{\mathrm{base}}(t')\,u_{\mathrm{stress}}(t'+t_s)\,\mathrm{d}t'}{\sqrt{\int_{t_1}^{t_2} u_{\mathrm{base}}^2(t')\,\mathrm{d}t' \cdot \int_{t_1}^{t_2} u_{\mathrm{stress}}^2(t')\,\mathrm{d}t'}}. \tag{3}$$

A two-step procedure is used: (i) estimate a global stretch factor Λ by maximising the correlation over scaled time axes; de-stretch u_{stress} accordingly; (ii) compute the residual fixed shift Δt by maximising R over pure time shifts. Both quantities are averaged over the burst support windows.

The optimal time shift t_s that maximises the correlation is plotted against the window centre t_c, and the local velocity change follows $\Delta v/v = -t_s^*/t_c$. The stretch factor is obtained from the slope of this relation. In our implementation, a global stretch is first determined by maximising equation (4) over scaled time axes and u_{stress} is de-stretched accordingly. A second CWI pass on the de-stretched signal then yields the residual fixed shift. This two-step procedure provides a robust and unique pair of observables–stretch and shift–from a single Rayleigh trace.

3 Results

Shift and stretch are governed by both surface stress and stress gradient. Applying the adapted CWI directly to the Rayleigh wave signal provides two observables from a single trace. Figure 3 isolates the effect of the normalised gradient χ at fixed surface stress σ_1. The shift Δt decreases as tensile stress increases (reduced velocity) and increases under compression (increased velocity). For a given σ_1, a larger χ systematically reduces the absolute shift, i.e., gradients bias the ToF toward smaller total time shifts $|\Delta t|$.

The time shift Δt is observed to follow

$$\Delta t = (K_0 + K_1\chi)\sigma_1 = K_0\sigma_{\mathrm{eff}}. \tag{4}$$

K_0 represents the acoustoelastic constant and thus quantifies the sensitivity of the wave velocity to a homogeneous stress state. K_1 accounts for the additional influence of the normalised stress gradient. K_1 can be regarded as a gradient-dependent acoustoelastic constant where K_0 is the acoustoelastic constant and K_1 is a corrective term for the influence of the stress gradient, with $R^2 \approx 0.996$. This confirms that gradients systematically reduce the absolute time shift for a given surface stress. We define the effective measured stress as the stress of a hypothetical gradient-free (uniform) state that results in the same total shift as the true stress state. If the stress distribution is known, the effective stress depth follows from

$$\sigma_{\mathrm{eff}} = \frac{1}{t_{\mathrm{eff}}}\int_0^{t_{\mathrm{eff}}} \sigma(z)\mathrm{d}z, \tag{5}$$

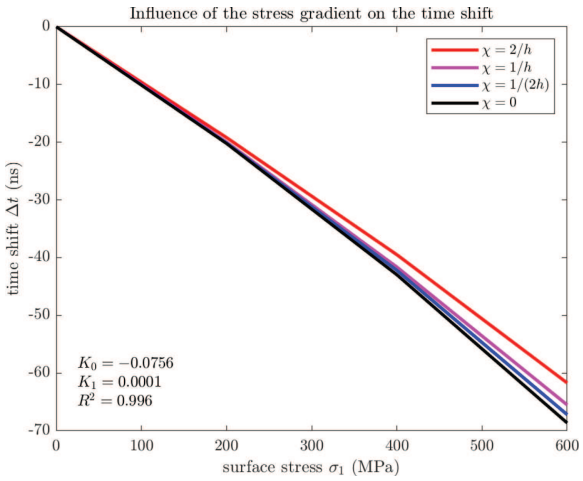

Figure 3. Influence of different normalised stress gradients on the total shift for same surface stresses.

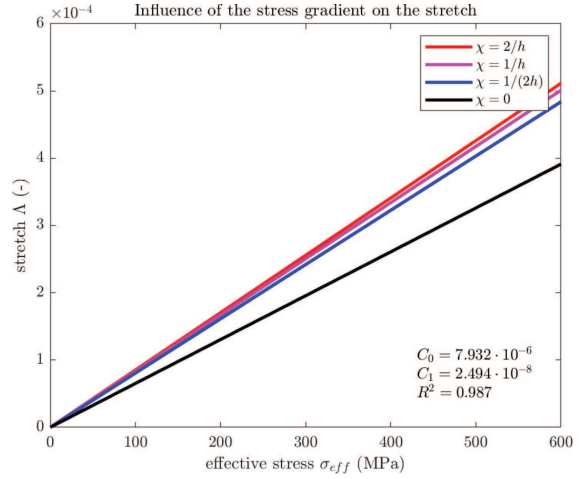

Figure 4. Influence of different stress distributions on the resulting stretch of elastic surface waves as a function of the effective stress.

where t_{eff} is the depth where the effective measured stress acts. It can be shown that $t_{\text{eff}} = \frac{2K_1}{K_0}$. Figure 4 plots the stretch Λ as a function of the effective stress σ_{eff} for several normalised stress gradients χ. For a homogeneous profile ($\chi = 0$), Λ attains its minimum, whereas the largest gradient yields the maximum Λ. Overall, at fixed σ_{eff} the stretch increases monotonically with χ, consistent with gradient-induced dispersion of the Rayleigh wave.

The stretch Λ, which quantifies waveform distortion due to depth-varying velocity, is well described by

$$\Lambda = (C_0 + C_1\chi)\,\sigma_{\text{eff}}, \qquad \sigma_{\text{eff}} = \frac{\Delta t}{K_0}, \tag{6}$$

with $R^2 \approx 0.987$. C_0 and C_1 are model constants. Coefficients K_0, K_1, C_0, C_1 are obtained by regression from FE datasets.

4 Discussion

Our simulations clarify how stress and, in particular, its depth gradient govern Rayleigh wave propagation. Two robust trends emerge and are internally consistent across all cases studied: (i) increasing tensile stress reduces the Rayleigh velocity (negative shift), and (ii) a positive gradient increases the apparent velocity, which manifests as a smaller absolute time shift for the same surface stress (Fig. 3). In parallel, the waveform distortion captured by the stretch grows with the normalised gradient χ at fixed effective stress (Fig. 4). Together, these observations explain why classical time-of-flight (ToF) evaluations that ignore gradients can bias near-surface residual-stress estimates. The results further indicate that the classical TOF method measures the effective stress– rather than the surface or the average stress within the propagation depth.

The gradient effect can be interpreted as a depth-weighting phenomenon: the measured signal integrates a stress-dependent velocity over the sampling region so that a tensile surface stress combined with a positive gradient yields a lower depth-averaged stress and, hence, a higher apparent velocity. This is captured by the compact regressions used here, where the gradient contribution gains weight as frequency decreases. Conversely, the influence of a homogeneous stress state on the observed timing over the MHz band is small compared to the gradient-driven effect seen in Λ.

Using the adapted CWI, we extract two trace-level observables that respond differently to the stress field: the shift follows $\Delta t = (K_0 + K_1\chi)\sigma_1$ and the stretch follows $\Lambda = (C_0 + C_1\chi)\sigma_{\text{eff}}$ with $\sigma_{\text{eff}} = \Delta t/K_0$. This pairing resolves the identifiability problem inherent to shift-only methods: combining Δt and Λ in a minimal inversion allows separation of surface stress and gradient and yields a concise, frequency-aware reconstruction workflow suitable for short-measurement campaigns.

Our simulations reveal that the penetration depth of Rayleigh waves is inherently frequency-dependent. Two consistent findings emerge: (i) the model parameters K_2 and C_2 vary systematically with excitation frequency, and (ii) this frequency dependence governs the apparent propagation velocity through the effective penetration depth. Together, these insights explain why analyses assuming constant K_2 and C_2 may lead to biased inversions. Consequently, solving the inverse problem requires an explicit determination of the frequency-dependent behaviour of $K_2(f)$ and $C_2(f)$.

The study assumes isotropy and a weakly nonlinear Murnaghan law; prior plastic deformation and anisotropy are represented only via effective constants. Linear stress profiles are considered; higher-order gradients and microstructural heterogeneity are not resolved. Numerical dispersion and finite-domain effects were mitigated but cannot be fully excluded. Future work will calibrate the coefficients on well-characterised specimens, extend the framework to anisotropic or textured materials, and validate the two-observable inversion on experimental

data across multiple frequencies and representative stress profiles.

5 Conclusion

This short communication numerically quantified how stress gradients govern Rayleigh wave propagation and showed how an adapted coda-wave interferometry can extract two complementary observables–shift and stretch–from a single surface trace. Based on FE simulation using Murnaghans hyperelastic material model, we found that tensile stress decreases, while stress gradients increase the apparent Rayleigh velocity; gradients also induce measurable dispersion. Compact regressions link shift and stretch to surface/effective stress and gradient, enabling a straightforward inversion that introduces the practical notions of effective measured stress and stress gradient. This approach provides a concise route to separate stress from gradient and to reconstruct near-surface residual-stress profiles. Future work should focus on experimental calibration (temperature/roughness), anisotropy and microstructural effects, and multi-frequency validation on reference specimens.

Acknowledgments

The authors thank the Austrian Research Promotion Agency (FFG) for financial support in project FO999899048.

Funding

The research was funded by the Austrian Research Promotion Agency (FFG) in project FO999899048.

Conflicts of interest

The authors declare no conflict of interest.

Data availability statement

The data is available on request by the authors.

Author contribution statement

Conceptualization (Marcel Ruetz), Data curation (Marcel Ruetz), Formal analysis (Marcel Ruetz), Funding acquisition (Hans-Peter Gänser), Investigation (Marcel Ruetz), Methodology (Marcel Ruetz), Project administration (Hans-Peter Gänser), Resources (Hans-Peter Gänser), Software (Marcel Ruetz), Supervision (Thomas Antretter & Hans-Peter Gänser), Validation (Marcel Ruetz), Visualization (Marcel Ruetz), Writing – original draft (Marcel Ruetz), Writing – review & editing (Marcel Ruetz & Thomas Antretter & Hans-Peter Gänser).

References

1. F.D. Murnaghan: Finite deformations of an elastic solid. American Journal of Mathematics 59 (1937) 235–260.
2. D.S. Hughes, J.L. Kelly: Second-order elastic deformation of solids. Physical Review 92 (1953) 1145–1149.
3. M. Hayes, R.S. Rivlin: Propagation of a plane wave in an isotropic elastic material subjected to pure homogeneous deformation. Archive for Rational Mechanics and Analysis 8 (1961) 15–22.
4. R.A. Toupin, B. Bernstein: Sound waves in deformed perfectly elastic materials. Acoustoelastic effect. Journal of the Acoustical Society of America 33 (1961) 216–225.
5. M. Ruetz, T. Antretter, H.-P. Gänser: Numerical investigation of the influence of the stress multiaxiality on the propagation behavior of Rayleigh waves. Applied Sciences 15, 16 (2025) 9109.
6. D.I. Crecraft: The measurement of applied and residual stresses in metals using ultrasonic waves. Journal of Sound and Vibration 5 (1967) 173–192.
7. T. Leon-Salamanca: Ultrasonic measurement of residual stress in steels using critically refracted longitudinal waves (LCR), Texas A & M University, Department of Mechanical Engineering, 1988.
8. M. Srinivasan, D.E. Bray, P. Junghans, A. Alagarsamy: Critically Refracted Longitudinal Waves Technique: a New Tool for the Measurement of Residual Stresses in Castings. Vol. 99. AFS (American Foundrymen Society), 1991.
9. C. Bescond, J.-P. Monchalin, D. Levesque, A. Gilbert, R. Talbot: Determination of residual stresses using laser-generated surface skimming longitudinal waves, in: Nondestructive Evaluation and Health Monitoring of Aerospace Materials, Composites, and Civil Infrastructure IV. Proceedings of the SPIE. Vol. 5767, 2005. doi: 10.1117/12.620374.
10. M.O. Si-Chaib, S. Menad, H. Djelouah, M. Bocquet: An ultrasound method for the acoustoelastic evaluation of simple bending stresses. NDT & E International 34 (2001) 521–529.
11. M.O. Si-Chaib, H. Djelouah, T. Boutkedjrt: Propagation of ultrasonic waves in materials under bending forces. NDT & E International 38 (2005) 283–289.
12. Y. Ivanova, T. Partalin: Investigation of stress-state in rolled sheets by ultrasonic techniques. Ultrasound 66, 1 (2011) 7–15.
13. R. Snieder: The theory of coda wave interferometry. Pure and Applied Geophysics 163, 2–3 (2006) 455–473.
14. R. Snieder, A. Gret, H. Douma, J. Scales: Coda wave interferometry for estimating nonlinear behavior in seismic velocity. Science 295, 5563 (2002) 2253–2255.
15. E. Siebel, M. Stieler: Dissimilar stress distributions and cyclic loading. Zeitschrift des Vereines Deutscher Ingenieure 97 (1955) 121–131.

Cite this article as: Ruetz M. Antretter T. & Gänser H.-P. 2026. On the influence of the stress gradient on propagation behaviour of Rayleigh waves. Acta Acustica, **10**, 27. https://doi.org/10.1051/aacus/2026028.